

# Constraints on Cosmological Parameters from the Ly $\alpha$ Forest Power Spectrum and COBE-DMR

John Phillips<sup>1</sup>, David H. Weinberg<sup>2</sup>,  
Rupert A. C. Croft<sup>2,3</sup>, Lars Hernquist<sup>3,4</sup>, Neal Katz<sup>5</sup>, and Max Pettini<sup>6</sup>

## ABSTRACT

We combine COBE-DMR measurements of cosmic microwave background (CMB) anisotropy with a recent measurement of the mass power spectrum at redshift  $z = 2.5$  from Ly $\alpha$  forest data to derive constraints on cosmological parameters and test the inflationary cold dark matter (CDM) scenario of structure formation. By treating the inflationary spectral index  $n$  as a free parameter, we are able to find successful fits to the COBE and Ly $\alpha$  forest constraints in  $\Omega_m = 1$  models with and without massive neutrinos and in low- $\Omega_m$  models with and without a cosmological constant. Within each class of model, the combination of COBE and the Ly $\alpha$  forest  $P(k)$  constrains a parameter combination of the form  $\Omega_m h^\alpha n^\beta \Omega_b^\gamma$ , with different indices for each case. This new constraint breaks some of the degeneracies in cosmological parameter determinations from other measurements of large scale structure and CMB anisotropy. The Ly $\alpha$  forest  $P(k)$  provides the first measurement of the slope of the linear mass power spectrum on  $\sim$  Mpc scales,  $\nu = -2.25 \pm 0.18$ , and it confirms a basic prediction of the inflationary CDM scenario: an approximately scale-invariant spectrum of primeval fluctuations ( $n \approx 1$ ) modulated by a transfer function that bends  $P(k)$  towards  $k^{n-4}$  on small scales. Considering additional observational data, we find that COBE-normalized,  $\Omega_m = 1$  models that match the Ly $\alpha$  forest  $P(k)$  do not match the observed masses of rich galaxy clusters and that low- $\Omega_m$  models with a cosmological constant provide the best overall fit to the available data, even without the direct evidence for cosmic acceleration from Type Ia supernovae. With our fiducial parameter choices, the flat, low- $\Omega_m$  models that match COBE and the Ly $\alpha$  forest  $P(k)$  also match recent measurements of small scale CMB anisotropy. Modest improvements in the Ly $\alpha$  forest  $P(k)$  measurement could greatly restrict the allowable region of

---

<sup>1</sup>Department of Physics, The Ohio State University, Columbus, OH 43210; phillips@pacific.mps.ohio-state.edu

<sup>2</sup>Department of Astronomy, The Ohio State University, Columbus, OH 43210; dhw@astronomy.ohio-state.edu

<sup>3</sup>Harvard-Smithsonian Center for Astrophysics, Cambridge, MA 02138; rcroft,lars@cfa.harvard.edu

<sup>4</sup>Lick Observatory, University of California, Santa Cruz, CA 95064

<sup>5</sup>Department of Physics and Astronomy, University of Massachusetts, Amherst, MA, 01003; nsk@kaka.phast.umass.edu

<sup>6</sup>Institute of Astronomy, Madingley Road, Cambridge, CB3 0HA, UK; pettini@ast.cam.ac.uk

parameter space for CDM models, constrain the contribution of tensor fluctuations to CMB anisotropy, and achieve a more stringent test of the current consensus model of structure formation.

## 1. Introduction

Cosmological models based on cold dark matter (CDM) and simple versions of inflation have had considerable success in accounting for the origin of cosmic structure. In this class of models, the primordial density fluctuations are Gaussian distributed, and the shape of their power spectrum is determined by a small number of physical parameters that describe the inflationary fluctuations themselves and the material contents of the universe. For specified cosmological parameters, the measurement of cosmic microwave background (CMB) anisotropies by the COBE-DMR experiment (Smoot et al. 1992; Bennett et al. 1996) fixes the amplitude of the matter power spectrum on large scales with an uncertainty of  $\sim 20\%$  (e.g., Bunn & White 1997). In this paper, we combine the COBE normalization with a recent measurement of the matter power spectrum by Croft et al. (1999b, hereafter CWPHK) to test the inflation+CDM scenario and constrain its physical parameters. A modified version of the method developed here is applied to a more recent power spectrum measurement by Croft et al. (2001).

CWPHK infer the mass power spectrum  $P(k)$  from measurements of Ly $\alpha$  forest absorption in the light of background quasars, at a mean absorption redshift  $z \approx 2.5$ . The method, introduced by Croft et al. (1998), is based on the physical picture of the Ly $\alpha$  forest that has emerged in recent years from 3-dimensional, hydrodynamic cosmological simulations and related analytic models (e.g., Cen et al. 1994; Zhang, Anninos, & Norman 1995; Hernquist et al. 1996; Bi & Davidsen 1997; Hui, Gnedin, & Zhang 1997). By focusing on the absorption from diffuse intergalactic gas in mildly non-linear structures, this method sidesteps the complicated theoretical problem of biased galaxy formation; it directly estimates the linear theory mass power spectrum (over a limited range of scales) under the assumption of Gaussian initial conditions. Because the observational units are  $\text{km s}^{-1}$ , the CWPHK measurement probes somewhat different comoving scales for different cosmological parameters:  $\lambda \equiv 2\pi/k = 2 - 12h^{-1}\text{Mpc}$  for  $\Omega_m=1$ ,  $\lambda = 3 - 16h^{-1}\text{Mpc}$  for  $\Omega_m=0.55$  and  $\Omega_\Lambda=0$ , and  $\lambda = 4 - 22h^{-1}\text{Mpc}$  for  $\Omega_m=0.4$  and  $\Omega_\Lambda=0.6$  ( $h \equiv H_0/100 \text{ km s}^{-1} \text{ Mpc}^{-1}$ ). CWPHK determine the logarithmic slope of  $P(k)$  on these scales with an uncertainty  $\sim 0.2$  and the amplitude with an uncertainty  $\sim 35\%$ . The extensive tests on simulations in Croft et al. (1998) and CWPHK suggest that the statistical uncertainties quoted here dominate over systematic errors in the method itself, though the measurement does depend on the assumption of Gaussian primordial fluctuations and on the broad physical picture of the Ly $\alpha$  forest described in the references above. For brevity, we will usually refer to the CWPHK determination of the mass power spectrum as “the Ly $\alpha$   $P(k)$ .”

In the next Section, we discuss our choice of the parameter space for inflationary CDM

models. The core of the paper is Section 3, where we combine the COBE normalization with the Ly $\alpha$   $P(k)$  to identify acceptable regions of the CDM parameter space. We focus on four representative models: a low density ( $\Omega_m < 1$ ) open model, a low density flat model with a cosmological constant, and Einstein-de Sitter ( $\Omega_m = 1$ ) models with pure CDM and with a mixture of CDM and hot dark matter. Because different parameters have nearly degenerate influences on the predicted Ly $\alpha$   $P(k)$ , we are able to summarize our results in terms of simple equations that constrain combinations of these parameters. In Section 4, we consider other observational constraints that can break these degeneracies, such as the cluster mass function, the peculiar velocity power spectrum, the shape of the galaxy power spectrum, and the CMB anisotropy power spectrum. We review our conclusions in Section 5.

## 2. Parameter Space for CDM Models

In simple inflationary models, the power spectrum of density fluctuations in the linear regime can be well approximated as a power law,  $P(k) \propto k^n$  (where  $n = 1$  is the scale-invariant spectrum), multiplied by the square of a transfer function  $T(k)$  that depends on the relative energy densities of components with different equations of state. We will assume the standard radiation background (microwave background photons and three species of light neutrinos) and consider as other possible components cold dark matter, baryons, a “cosmological constant” vacuum energy, and neutrinos with a non-zero rest mass in the few eV range. Within this class of models, the shape of the power spectrum is therefore determined by the parameters  $n$ ,  $\Omega_{\text{CDM}}$ ,  $\Omega_b$ ,  $\Omega_\Lambda$ ,  $\Omega_\nu$ , and  $h$  (since  $\rho_x = \Omega_x \rho_c \propto \Omega_x h^2$ ). In place of  $\Omega_b$  and  $\Omega_{\text{CDM}}$ , we use the parameters

$$B \equiv \Omega_b h^2, \tag{1}$$

which is constrained by light-element abundances through big bang nucleosynthesis (Walker et al. 1991), and

$$\Omega_m \equiv \Omega_{\text{CDM}} + \Omega_b + \Omega_\nu, \tag{2}$$

which fixes  $\Omega_{\text{CDM}}$  once  $B$ ,  $h$ , and  $\Omega_\nu$  are specified. For non-zero  $\Omega_\nu$ , we assume one dominant family of massive neutrinos. We do not consider arbitrary combinations of  $\Omega_m$  and  $\Omega_\Lambda$  but instead restrict our attention to the two theoretically simplest possibilities, spatially flat models with  $\Omega_\Lambda = 1 - \Omega_m$  and open models with  $\Omega_\Lambda = 0$ .

Once the cosmological parameters are specified, normalizing to the results of the COBE-DMR experiment determines the amplitude of  $P(k)$ . For inflation models with  $n < 1$ , the COBE normalization can also be affected by the presence of tensor fluctuations (gravity waves). We consider normalizations with no tensor contribution and normalizations with the quadrupole tensor-to-scalar ratio  $T/S = 7(1 - n)$  predicted by simple power law inflation models (e.g., Davis et al. 1992), but we do not consider arbitrary tensor contributions. We compute the COBE-normalized, linear theory, matter power spectrum  $P(k)$  using the convenient and accurate

fitting formulas of Eisenstein & Hu (1999), with the normalization procedures of Bunn & White (1997) for all flat cases and for the open case without a tensor contribution and Hu & White (1997) for the open case with a tensor contribution.

There are plausible variants of this family of inflationary CDM models that we do not analyze in this paper, because we lack the tools to easily calculate their predictions and because they would make our parameter space intractably larger. Prominent among these variants are models with a time-varying scalar field, a.k.a. “quintessence” (e.g., Peebles & Ratra 1988; Wang & Steinhardt 1998), models in which the energy of the radiation background has been boosted above its standard value by a decaying particle species, a.k.a. “ $\tau$ CDM” (e.g., Bond & Efstathiou 1991), and models in which inflation produces a power spectrum with broken scale invariance (e.g., Kates et al. 1995). Given the observational evidence for a negative pressure component from Type Ia supernovae (Riess et al. 1998; Perlmutter et al. 1999), the quintessence family might be especially interesting to explore in future work.

In sum, the free parameters of our family of cosmological models are  $\Omega_m$ ,  $h$ ,  $n$ ,  $B$ ,  $\Omega_\nu$ ,  $\Omega_\Lambda$ , and  $T/S$ . We allow  $\Omega_m$ ,  $h$ ,  $n$ ,  $B$ , and  $\Omega_\nu$  to assume a continuous range of values. For  $\Omega_\Lambda$  and  $T/S$  we consider only two discrete options:  $\Omega_\Lambda = 0$  or  $1 - \Omega_m$ , and  $T/S = 0$  or  $7(1 - n)$ .

### 3. Cosmological Parameters and the Ly $\alpha$ Forest $\mathbf{P}(\mathbf{k})$

To organize our discussion and guide our analysis, we focus on variations about four fiducial models, each motivated by a combination of theoretical and observational considerations. The fiducial models are a flat cold dark matter model with a non-zero cosmological constant ( $\Lambda$ CDM), an open cold dark matter model with no cosmological constant (OCDM), an  $\Omega_m = 1$  cold dark matter model with a significantly “tilted” inflationary spectrum (TCDM), and an  $\Omega_m = 1$  model with a mixture of cold and hot dark matter (CHDM).

For all of the fiducial models we adopt  $B = 0.02$ , based on recent measurements of the deuterium abundance in high-redshift Lyman limit absorbers (Burles & Tytler 1997, 1998). For the TCDM and CHDM models we adopt  $h = 0.5$  in order to obtain a reasonable age for the universe given the assumption that  $\Omega_m = 1$ . For the  $\Lambda$ CDM and OCDM models we instead adopt  $h = 0.65$ , which is better in line with recent direct estimates of the Hubble constant (e.g., Mould et al. 2000). For the  $\Lambda$ CDM model we take  $\Omega_m = 0.4$ , but for OCDM we adopt a rather high density,  $\Omega_m = 0.55$ , in anticipation of our results in Section 4, where we consider the cluster mass function as an additional observational constraint. For the CHDM model, we take  $\Omega_\nu = 0.2$  and assume one dominant species of massive neutrino; for all other models  $\Omega_\nu = 0$ . With  $B$ ,  $h$ ,  $\Omega_m$ , and  $\Omega_\nu$  fixed, we are left with one free parameter, the inflationary spectral index  $n$ , which we choose in order to fit the amplitude of the Ly $\alpha$   $P(k)$  while maintaining the COBE normalization. The required value of  $n$  is different for models with no tensor contribution to CMB anisotropies than for models with tensor fluctuations; we refer to the fiducial models with tensor fluctuations as

$\Lambda$ CDM2, OCDM2, and TCDM2. Because a value  $n > 1$  is required for CHDM and the assumption that  $T/S = 7(1 - n)$  therefore cannot be correct in this case, we do not consider a CHDM model with tensor fluctuations. Table 1 lists the parameters of the fiducial models. For later reference, Table 1 also lists each model’s value of  $\sigma_8$ , the rms linear theory mass fluctuation in spheres of radius  $8h^{-1}\text{Mpc}$  at  $z = 0$ .

Figure 1 compares the power spectra of our fiducial models to the Ly $\alpha$   $P(k)$ , shown as the filled circles with error bars. Note that the overall normalization of the data points is uncertain; at the  $1\sigma$  level they can shift up or down coherently by the amount indicated by the error bar on the open circle (see CWPBK for details). The COBE normalization itself has a  $1\sigma$  uncertainty of approximately 20% in  $P(k)$ , roughly half of the Ly $\alpha$   $P(k)$  normalization uncertainty. Panels (a) and (c) show the fiducial models with and without tensors, respectively, over a wide range of wavenumber. Panels (b) and (d) focus on the range of wavenumbers probed by the Ly $\alpha$   $P(k)$ . Our first major result is already evident from Figure 1: all of the fiducial models reproduce the observed Ly $\alpha$   $P(k)$ . Each model has a single adjustable parameter, the spectral index  $n$ , so their success in reproducing both the amplitude and slope of  $P(k)$  is an important confirmation of a generic prediction of the inflationary CDM scenario, a point we will return to shortly.

Within the precision and dynamic range of the CWPBK measurement, the Ly $\alpha$   $P(k)$  can be adequately described by a power law. CWPBK find

$$\Delta^2(k) \equiv \frac{k^3}{2\pi^2} P(k) = \Delta^2(k_p) \left( \frac{k}{k_p} \right)^{3+\nu}, \quad (3)$$

with

$$k_p = 0.008 (\text{km s}^{-1})^{-1}, \quad (4)$$

$$\Delta^2(k_p) = 0.573_{-0.166}^{+0.233}, \quad (5)$$

$$\nu = -2.25 \pm 0.18. \quad (6)$$

Here  $\Delta^2(k)$  is the contribution to the density variance per unit interval of  $\ln k$ , and  $k_p$  is a “pivot” wavenumber near the middle of the range probed by the data.

Table 1: Fiducial Models

Model	$\Omega_m$	$\Omega_\Lambda$	$h$	$n$	$B$	$\Omega_\nu$	T/S	$\sigma_8$
$\Lambda$ CDM	0.4	0.6	0.65	0.96	0.02	0.0	0	0.91
$\Lambda$ CDM2	0.4	0.6	0.65	0.98	0.02	0.0	$7(1 - n)$	0.89
OCDM	0.55	0.0	0.65	0.88	0.02	0.0	0	0.67
OCDM2	0.55	0.0	0.65	0.92	0.02	0.0	$7(1 - n)$	0.64
TCDM	1.0	0.0	0.50	0.84	0.02	0.0	0	0.77
TCDM2	1.0	0.0	0.50	0.89	0.02	0.0	$7(1 - n)$	0.73
CHDM	1.0	0.0	0.50	1.10	0.02	0.2	0	0.96

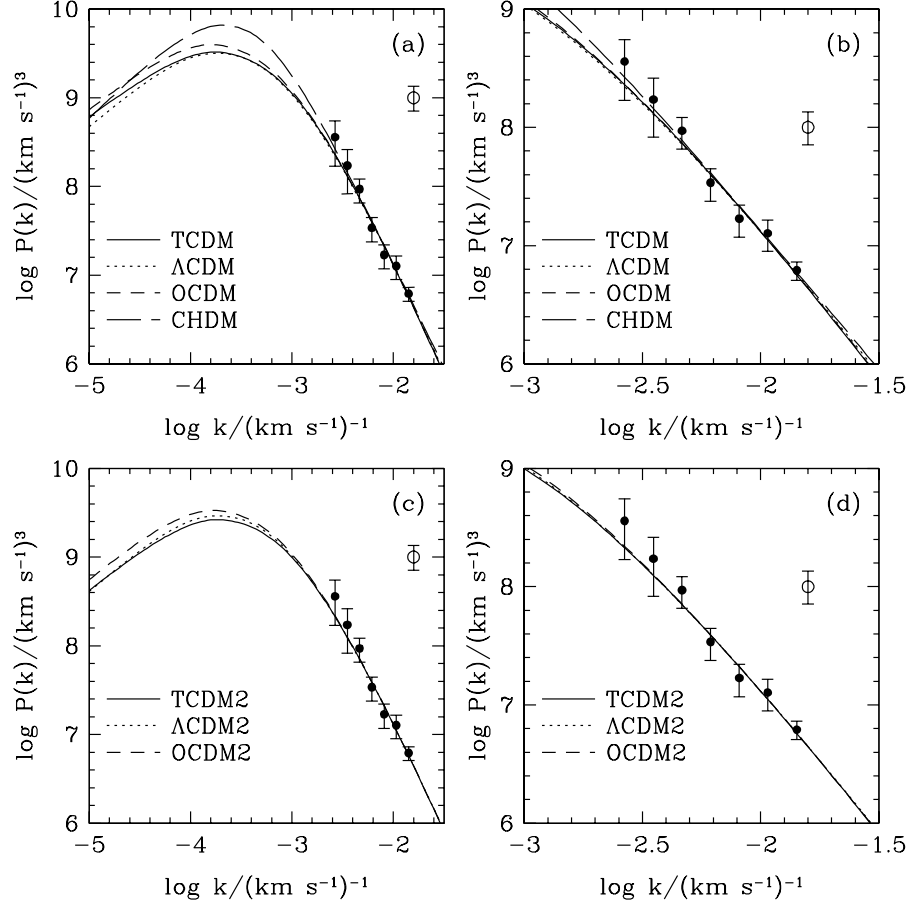


Fig. 1.— Power spectra of the fiducial models (smooth curves) compared to the Ly $\alpha$   $P(k)$  determined by CWPHK (filled circles). Upper panels show models with no tensor fluctuations and lower panels show models with tensor fluctuations; the right hand panels zoom in on the range of wavenumbers probed by the Ly $\alpha$   $P(k)$ . The error bar on the open circle shows an overall normalization uncertainty in the Ly $\alpha$   $P(k)$ ; at the  $1\sigma$  level all of the points can shift up or down coherently by this amount. Model parameters are listed in Table 1.

In each panel of Figures 2 and 3, the central star shows the best fit values of  $\Delta^2(k_p)$  and  $\nu$  quoted above, and the two large concentric circles show the  $1\sigma$  (68%) and  $2\sigma$  (95%) confidence contours on the parameter values. The calculation of these confidence contours is described in detail in Section 5 of CWPBK. Briefly, the likelihood distribution for the slope,  $\nu$ , is derived by fitting the power law form (eq. 3) to the  $P(k)$  data points, using their covariance matrix. The likelihood distribution for the amplitude,  $\Delta^2(k_p)$ , is obtained by convolving the distributions calculated from two separate sources of uncertainty involved in the  $P(k)$  normalization. The joint confidence contours on the two parameters are obtained by multiplying together the two independent likelihood distributions. The  $1\sigma$  and  $2\sigma$  contours correspond to changes in  $-2\log_e \mathcal{L}$  from its best fit value of 2.30 and 6.17, respectively, where  $\mathcal{L}$  is the likelihood.

The open circular point near the middle of each panel of these figures shows the fiducial model’s prediction of  $\Delta^2(k_p)$  and  $\nu$ .  $\Lambda$ CDM, OCDM, and TCDM models without tensors appear in the left column of Figure 2, the corresponding models with tensors appear in the right column of Figure 2, and the CHDM model appears in Figure 3. As expected from Figure 1, the fiducial model predictions lie well within the 68% confidence contour in all cases. The 20% COBE normalization uncertainty adds a  $\log(1.2) \approx 0.08$  error bar to the predicted value of  $\log \Delta^2(k_p)$ , which we have not included in the plots. Because this uncertainty is small (once added in quadrature) compared to the Ly $\alpha$   $P(k)$  uncertainty itself, we have ignored it in the analysis of this paper. With a higher precision Ly $\alpha$  forest measurement, it would be important to include the COBE normalization uncertainty as an additional source of statistical error.

Changing any of the parameter values in any of the models shifts the predicted  $\Delta^2(k_p)$  and  $\nu$ , and the remaining points in Figures 2 and 3 show the effects of such parameter changes. Taking the  $\Lambda$ CDM model of Figure 2a as an example, the two filled circles show the effect of increasing  $\Omega_m$  by 0.1 and 0.2 (to  $\Omega_m = 0.5$  and  $\Omega_m = 0.6$ ), while maintaining the condition  $\Omega_m + \Omega_\Lambda = 1$  and keeping all other parameters fixed at the fiducial values listed in Table 1. The two open circles show the effect of decreasing  $\Omega_m$  by 0.1 and 0.2. With  $\Omega_m = 0.2$  and other parameters unchanged (leftmost open circle), the predicted amplitude  $\Delta^2(k_p)$  falls below the 95% confidence lower limit of CWPBK. In similar fashion, filled (open) pentagons show the effect of increasing (decreasing)  $n$  by 0.05, filled (open) squares show the effect of increasing (decreasing)  $h$  by 0.05, and filled (open) triangles show the effect of increasing (decreasing)  $\Omega_b$  by 0.01, in all cases keeping the other parameters fixed at their fiducial values. The format of the other panels of Figure 2 is identical, except that we do not show  $\Omega_m$  changes for TCDM. For  $\Lambda$ CDM2 and OCDM2, we do not allow  $n > 1$ . In Figure 3, filled (open) hexagons show the effect of increasing (decreasing)  $\Omega_\nu$  by 0.1 while keeping  $\Omega_m = 1$ . Open circles show the effect of decreasing  $\Omega_m$  by 0.1 while adding  $\Omega_\Lambda$  to maintain flat space; results are virtually indistinguishable if  $\Omega_\Lambda$  is zero and the universe becomes (slightly) open. We do not consider changes that make  $\Omega_m > 1$ .

Parameter changes have similar effects in all of the models, and these effects can be easily understood by considering the physics that determines the shape and normalization of the matter power spectrum. The CDM transfer function has a single fundamental scale  $ct_{\text{eq}}$  determined

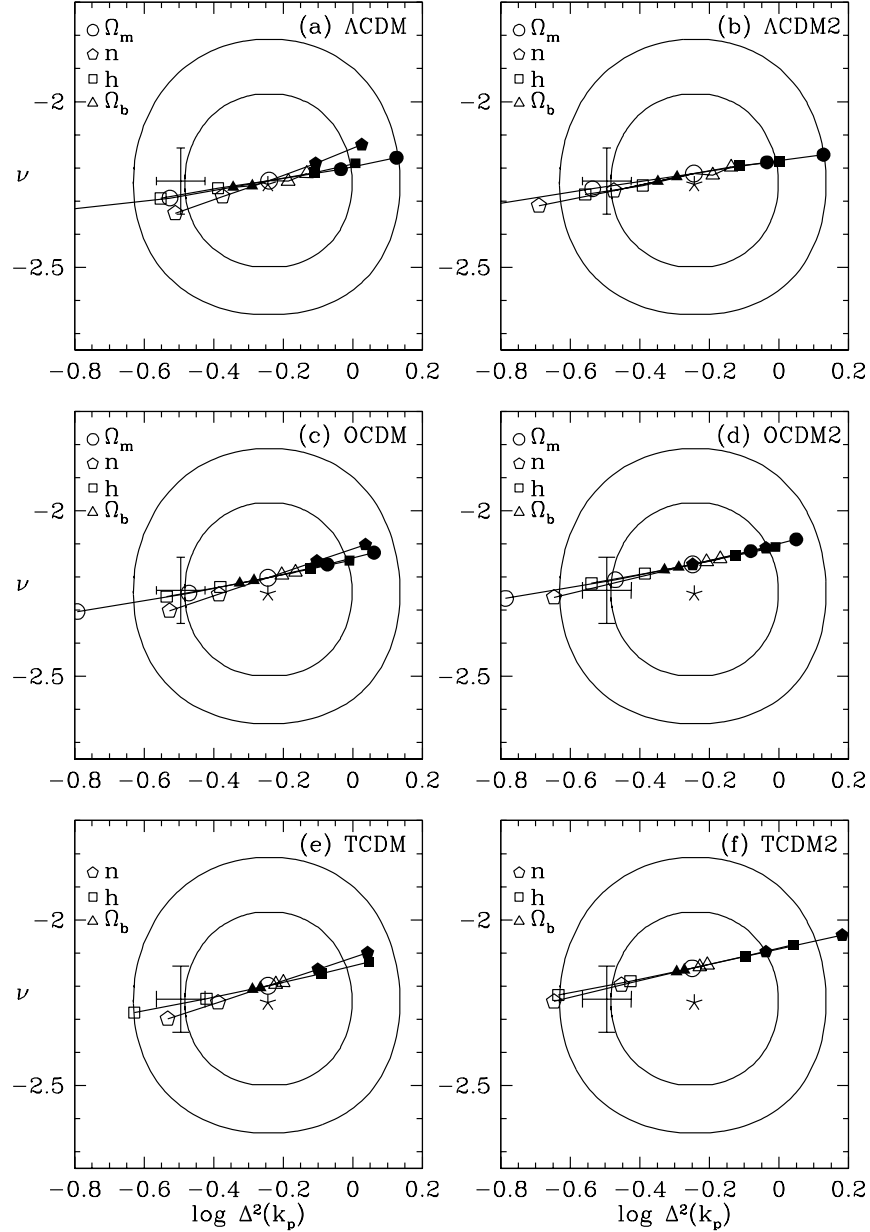


Fig. 2.— Constraints on the parameters of CDM models from COBE and the Ly $\alpha$   $P(k)$  measurement. In each panel, the central star shows CWPHK’s best-fit values of  $\Delta^2(k_p)$  and  $\nu$ , and closed contours show the 68% and 95% confidence regions. Each panel corresponds to a different one of the fiducial models, with the central open circle marking the model prediction for the parameters listed in Table 1. Other filled (open) points show the effects of increasing (decreasing) these parameters by fixed amounts while keeping all other parameters fixed. Circles show changes  $\Delta\Omega_m = 0.1$ , pentagons  $\Delta n = 0.05$ , squares  $\Delta h = 0.05$ , and triangles  $\Delta\Omega_b = 0.01$ ;  $\Omega_m$  changes are not considered for TCDM, and  $n > 1$  is not considered for models with tensor fluctuations. The error cross shows the Ly $\alpha$   $P(k)$  measurement of McDonald et al. (2000).



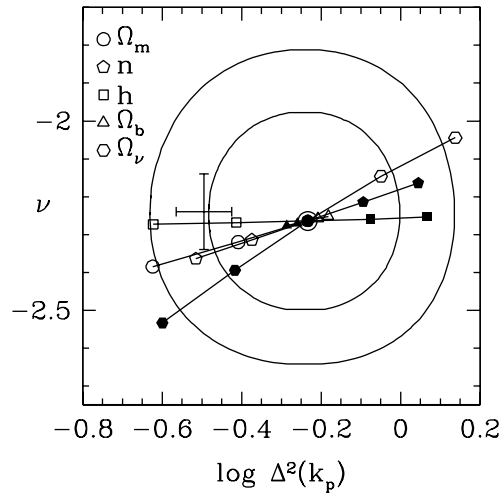


Fig. 3.— Like Figure 2, but for the CHDM model. Hexagons show changes of  $\Omega_\nu$  by  $\Delta\Omega_\nu = 0.1$ .

by the size of the horizon at the time of matter-radiation equality; this scale is roughly the wavelength at which the power spectrum turns over. Increasing  $h$ , and hence the matter density  $\rho_m \propto \Omega_m h^2$ , moves matter-radiation equality to higher redshift and lower  $t_{\text{eq}}$ , shifting the model power spectrum towards smaller scales (to the right in Figure 1). This horizontal shift, combined with an upward vertical shift to maintain the COBE normalization on large scales, increases the amplitude of  $P(k)$  on Ly $\alpha$  forest scales and translates a shallower (higher  $\nu$ ) part of the spectrum to  $k_p$ . Increasing  $\Omega_m$  also lowers  $t_{\text{eq}}$  and therefore has a similar effect. Open models are more sensitive than flat models to changes in  $\Omega_m$  because the integrated Sachs-Wolfe effect makes a greater contribution to large scale CMB anisotropies (Sachs & Wolfe 1967; Hu, Sugiyama, & Silk 1997). Increasing  $\Omega_m$  reduces the integrated Sachs-Wolfe effect and hence increases the matter fluctuation amplitude implied by COBE, shifting the power spectrum vertically upward. The value of  $\Delta^2(k_p)$  is sensitive to the spectral index  $n$  because of the very long lever arm between the COBE normalization scale and the scale of the Ly $\alpha$  forest measurement. A small decrease in  $n$  produces an equally small decrease in  $\nu$  but a large decrease in  $\Delta^2(k_p)$ . The fluctuation amplitude is even more sensitive to  $n$  in tensor models because, with  $T/S = 7(1 - n)$ , decreasing  $n$  also increases the contribution of gravity waves to the observed COBE anisotropies and therefore reduces the implied amplitude of the (scalar) matter fluctuations. Since fluctuations in the baryon component can only grow after the baryons decouple from the photons, increasing  $B$  depresses and steepens  $P(k)$  on small scales and therefore reduces  $\Delta^2(k_p)$  and  $\nu$ . However, for our adopted parameters the baryons always contribute a small fraction of the overall mass density, so the influence of  $\Omega_b$  changes is small. Increasing  $\Omega_\nu$  in the CHDM model has a much greater effect in the same direction, since the suppression of small scale power by neutrino free streaming is much greater than the suppression by baryon-photon coupling.

Figures 2 and 3 re-emphasize the point made earlier in our discussion of Figure 1: the agreement between the predicted and measured slope of the Ly $\alpha$   $P(k)$  confirms a general prediction of the inflationary CDM scenario. Although the four fiducial models correspond to quite different versions of this scenario, all of them reproduce the measured value of  $\nu = -2.25$  to well within its  $1\sigma$  uncertainty once the value of  $n$  is chosen to match the measured  $\Delta^2(k_p)$ . However, if the measured value of  $\nu$  had been substantially different, e.g. implying  $\nu > -2$  or  $\nu < -2.5$ , then none of these models could have reproduced the measured  $\nu$  while remaining consistent with the measured  $\Delta^2(k_p)$ , even allowing changes in  $n$ ,  $\Omega_m$ ,  $h$ ,  $\Omega_\nu$ , or  $\Omega_b$ . A different value of  $\nu$  would therefore have been a challenge to the inflationary CDM scenario itself rather than to any specific version of it. Note also that any of the models would match the observed  $\nu$  within its  $1\sigma$  uncertainty even if we had assumed a scale-invariant,  $n = 1$  inflationary spectrum; it is the  $\Delta^2(k_p)$  measurement that requires the departures from  $n = 1$ . Because of the long lever arm from COBE to the Ly $\alpha$   $P(k)$ , parameter changes that have a modest effect on  $\nu$  have a large effect on  $\Delta^2(k_p)$ .

Figure 2 also shows that changes of the different model parameters have nearly degenerate effects on the predicted values of  $\Delta^2(k_p)$  and  $\nu$ . For example, in the  $\Lambda$ CDM model, increasing  $\Omega_m$  by 0.1 would increase the predicted slope and amplitude, but decreasing  $h$  by 0.05 would almost

exactly cancel this change. This near degeneracy allows us to summarize the constraints imposed by COBE and the Ly $\alpha$   $P(k)$  with simple formulas of the form

$$\Omega_m h^\alpha n^\beta B^\gamma = k \pm \epsilon, \tag{7}$$

where  $k$  is the value obtained for the best-fit parameter values in Table 1 and the uncertainty  $\epsilon$  defines the variation that is allowed before the model leaves the 68% confidence contour. Table 2 lists the values of  $\alpha$ ,  $\beta$ ,  $\gamma$ ,  $k$ , and  $\epsilon$  for all of the fiducial models. Although we do not show  $\Omega_m$  changes for the TCDM models in Figure 2, we vary it below 1.0 (adding  $\Omega_\Lambda$  to keep the universe flat) in order to derive the  $\alpha$ ,  $\beta$ , and  $\gamma$  indices, so that in all models their values reflect the importance of a change in  $h$ ,  $n$ , or  $B$  relative to a change in  $\Omega_m$ .

Equation (7), together with Table 2, is our second principal result, defining the quantitative constraints placed on the parameters of inflationary CDM models by the combination of COBE and the Ly $\alpha$  forest  $P(k)$ . The values of the  $\alpha$ ,  $\beta$ , and  $\gamma$  indices reflect the sensitivity of the predicted power spectrum amplitude  $\Delta^2(k_p)$  to the model parameters, quantifying the impressions from Figure 2. Again taking  $\Lambda$ CDM as an example, we see that small variations in  $h$  and  $n$  have much greater effect than small variations in  $\Omega_m$ , and that the suppression of small scale power from increases in  $B$  is always a modest effect. Models with tensors are much more sensitive to  $n$  than models without tensors because of the influence of gravity waves on the  $P(k)$  normalization, as discussed above. Although the index values are derived in all cases by considering small variations about the corresponding fiducial model, the constraint formula (7) remains accurate even for fairly large changes in the cosmological parameters. For example, plugging the TCDM values of  $\Omega_m$ ,  $h$ ,  $n$ ,  $B$  into equation (7) with the  $\Lambda$ CDM values of  $\alpha$ ,  $\beta$ , and  $\gamma$  yields  $k = 0.47$ , compared to the value  $k = 0.44$  listed for  $\Lambda$ CDM in Table 2.

Figure 3 shows that the effects of parameter changes are less degenerate in the CHDM model. This difference in behavior is not surprising, since neutrino free streaming changes  $P(k)$  by depressing it at small scales rather than simply shifting or tilting it. The slope  $\nu$  is therefore much more sensitive to changes in  $\Omega_\nu$  than to changes in other parameters. Conversely, the influence of  $h$  on  $\nu$  through shifting  $t_{\text{eq}}$  is nearly cancelled by the effect of  $h$  on the implied neutrino mass and

Table 2: Constraint Parameters (see equation 7)

Model	$\alpha$	$\beta$	$\gamma$	$\delta$	$k$	$\epsilon$
$\Lambda$ CDM	1.88	2.68	-0.26	–	0.44	0.12
$\Lambda$ CDM2	1.84	4.48	-0.25	–	0.43	0.08
OCDM	1.55	2.57	-0.23	–	0.50	0.10
OCDM2	1.80	3.45	-0.18	–	0.38	0.08
TCDM	2.33	4.08	-0.40	–	0.46	0.14
TCDM2	1.82	4.60	-0.15	–	0.30	0.08
CHDM	0.93	1.74	-0.13	-0.37	1.87	0.26

free streaming length. We still analyze this case as above, adding a factor of  $\Omega_\nu^\delta$ , to obtain

$$\Omega_m h^\alpha n^\beta B^\gamma \Omega_\nu^\delta = k \pm \epsilon, \quad (8)$$

with parameters also listed in Table 1. However, this equation cannot describe the results of Figure 3 as accurately as equation (7) describes the results of Figure 2.

Recently McDonald et al. (2000) measured the Ly $\alpha$  forest flux power spectrum in a sample of eight Keck HIRES spectra and used it to infer the amplitude and shape of the mass power spectrum. Their mean absorption redshift is  $z \approx 3$  rather than  $z = 2.5$ , and their data best constrain the  $P(k)$  amplitude at  $k = 0.04 \text{ (km s}^{-1}\text{)}^{-1}$  rather than  $0.008 \text{ (km s}^{-1}\text{)}^{-1}$ . However, assuming gravitational instability and a CDM power spectrum shape, they extrapolate from their result to derive values of  $\nu$  and  $\Delta^2$  that can be directly compared to CWPHK’s measurement at  $z = 2.5$ ,  $k_p = 0.008 \text{ (km s}^{-1}\text{)}^{-1}$ , obtaining  $\nu = -2.24 \pm 0.10$  and  $\Delta^2(k_p) = 0.32 \pm 0.07$ . Despite the entirely independent data sets and very different modelling procedures, the CWPHK and McDonald et al. (2000) measurements agree almost perfectly in slope and are consistent in amplitude at the  $\sim 1\sigma$  level. We plot the McDonald et al. (2000) measurement as error crosses in Figures 2 and 3. McDonald et al. (2000) note that the small error bar on  $\Delta^2$  should be considered preliminary, since they have not fully investigated the sensitivity of their power spectrum normalization procedure to their modelling assumptions.

Clearly none of our qualitative conclusions about inflationary CDM models would change if we were to adopt the McDonald et al. (2000)  $P(k)$  determination instead of the CWPHK determination. Conveniently, the McDonald et al. (2000) point lies almost exactly on our  $-1\sigma$  error contour, so to a good approximation one can obtain the parameter constraints (7) and (8) implied by the McDonald et al. (2000) measurement by simply replacing the values of  $k$  in Table 2 by  $k - \epsilon$ .

#### 4. Combining with other constraints

We have shown that the combination of COBE and the Ly $\alpha$   $P(k)$  yields constraints on degenerate combinations of cosmological parameters. To break these degeneracies, we now consider observational constraints from other studies of large scale structure and CMB anisotropies. Analyses of cosmological parameter constraints from multiple observations have been carried out by numerous groups (recent examples include Bahcall et al. 1999; Bridle et al. 1999; Steigman, Hata, & Felten 1999; Novosyadlyj et al. 2000; Wang, Tegmark, & Zaldarriaga 2001). Our new contribution is to include the Ly $\alpha$   $P(k)$  as one of the observational constraints (also considered by Novosyadlyj et al. 2000 and Wang, Tegmark, & Zaldarriaga 2001). We focus our attention on several other constraints that can be cast into a form that complements our results from Section 3: the mass function of galaxy clusters, the mass power spectrum inferred from galaxy peculiar velocities, the shape parameter of the galaxy power spectrum, and a constraint on  $n$  from CMB anisotropy data. Our discussion in this Section will be more qualitative than our discussion in

Section 3, in part because the uncertainties in these constraints are largely systematic, so that a straightforward statistical combination could be misleading.

In each panel of Figures 4 and 5, the heavy solid line shows the locus of  $(\Omega_m, n)$  values that yield a simultaneous match to COBE and the CWPHK measurement of the Ly $\alpha$   $P(k)$ . These lines are very close to those implied by equation (7) and Table 2, but since those results are, strictly speaking, expansions about our fiducial model parameters, we compute the best-fit value of  $n$  exactly for each  $\Omega_m$  rather than using equation (7). The  $\pm 1\sigma$  constraints are shown as the lighter solid lines; these are close to the curves implied by equation (7) and Table 2 with  $k$  replaced by  $k \pm \epsilon$ . Because the Ly $\alpha$   $P(k)$  constraint is not very sensitive to  $B$ , we keep  $B$  fixed at our fiducial value of 0.02 in all cases. We show results for  $h = 0.65$ ,  $h = 0.45$ , and  $h = 0.85$  in the upper, middle, and lower panels of each figure, with flat and open models in the left and right hand columns, respectively. Figure 4 shows models without tensors and Figure 5 models with tensors. For models with tensors, we restrict the parameter space to  $n \leq 1$ , since our assumption that  $T/S = 7(1 - n)$  only makes sense in this regime. The TCDM models can be considered as the limit of either the flat or open models at  $\Omega_m = 1$ . Note that the McDonald et al. (2000) estimate of the Ly $\alpha$   $P(k)$  corresponds very closely to our  $-1\sigma$  constraint, so to adopt McDonald et al. (2000) instead of CWPHK one simply follows the lower solid line instead of the middle solid line as the constraint.

For Gaussian initial conditions, the space density of clusters as a function of virial mass constrains a combination of  $\Omega_m$  and the mass fluctuation amplitude, since clusters of a given mass can be formed by the collapse of large volumes in a low density universe or smaller volumes in a higher density universe. This constraint can be summarized quite accurately in a formula relating  $\Omega_m$  to the rms mass fluctuation  $\sigma_8$  (White, Efstathiou, & Frenk 1993a). We use the specific version of this formula obtained by Eke, Cole, & Frenk (1996, hereafter ECF) using N-body simulations and the Press-Schechter (1974) approximation:

$$\begin{aligned} \sigma_8 &= (0.52 \pm 0.04)\Omega_m^{-0.46+0.10\Omega_m} & \Omega_\Lambda &= 0 \\ \sigma_8 &= (0.52 \pm 0.04)\Omega_m^{-0.52+0.13\Omega_m} & \Omega_\Lambda &= 1 - \Omega_m . \end{aligned} \tag{9}$$

For each value of  $\Omega_m$ , we find the value of  $\sigma_8$  required by the cluster mass function from equation (9). Given  $h$  and  $B = 0.02$ , we then find the value of  $n$  required to produce this value of  $\sigma_8$  by numerically integrating the CDM power spectrum. This constraint in the  $\Omega_m - n$  plane is shown by the dotted line in each panel of Figures 4 and 5, with an error bar that indicates the 8% uncertainty quoted in equation (9) from ECF.

For a given value of  $\Omega_m$ , the matter power spectrum can also be estimated from the statistics of galaxy peculiar motions. Freudling et al. (1998) apply a maximum likelihood technique to the SFI peculiar velocity catalog to constrain COBE-normalized, inflationary CDM models for the matter power spectrum, obtaining the constraint

$$\Omega_m h_{60}^\mu n^\nu = k \pm \epsilon , \tag{10}$$

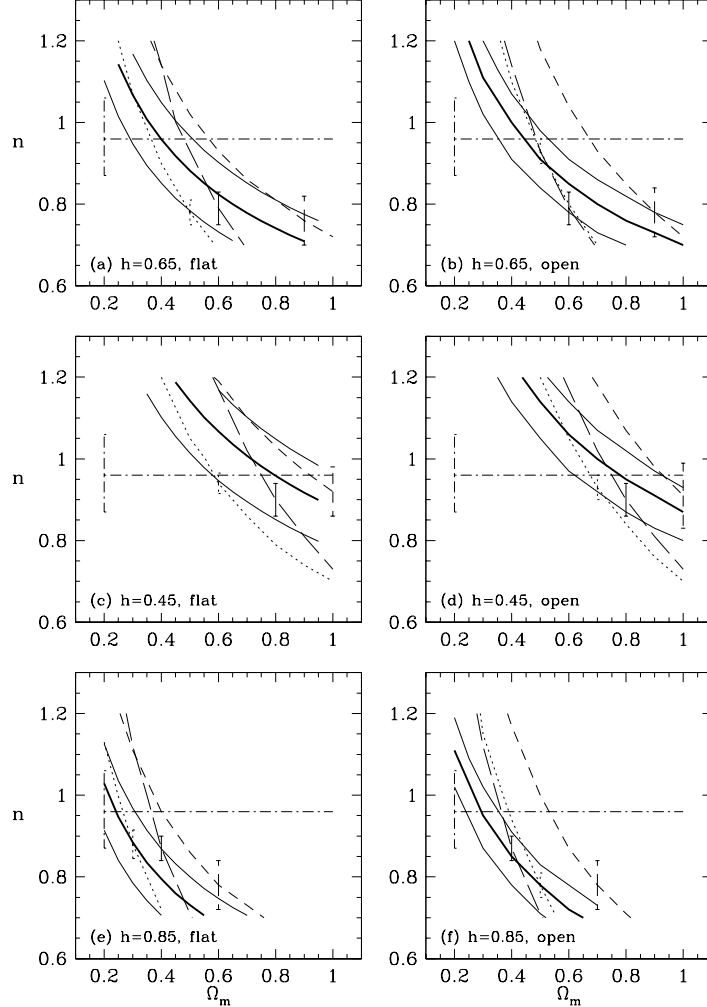


Fig. 4.— Constraints in the  $\Omega_m - n$  plane from a variety of cosmological tests, for models with no tensor fluctuations. Upper, middle, and lower panels show models with  $h = 0.65$ ,  $h = 0.45$ , and  $h = 0.85$ , respectively, and in all cases we keep  $B = 0.02$ . Flat models appear in the left hand column, open models with  $\Omega_\Lambda = 0$  in the right hand column. In each panel, the heavy solid line shows the  $\Omega_m - n$  locus determined by the combination of COBE and the Ly $\alpha$   $P(k)$ , and the light solid lines show the  $\pm 1\sigma$  range of this locus. Dotted lines show the constraint (9) from the cluster mass function, short-dashed lines the constraint (10) from the peculiar velocity power spectrum, long-dashed lines the constraint (11) from the shape of the galaxy power spectrum, and horizontal dot-dashed lines the constraint on  $n$  from CMB anisotropy measurements. Error bars show representative  $1\sigma$  statistical uncertainties in these constraints. A model is consistent with multiple constraints if it lies in the region of the  $\Omega_m - n$  plane where these constraints overlap within their uncertainties.

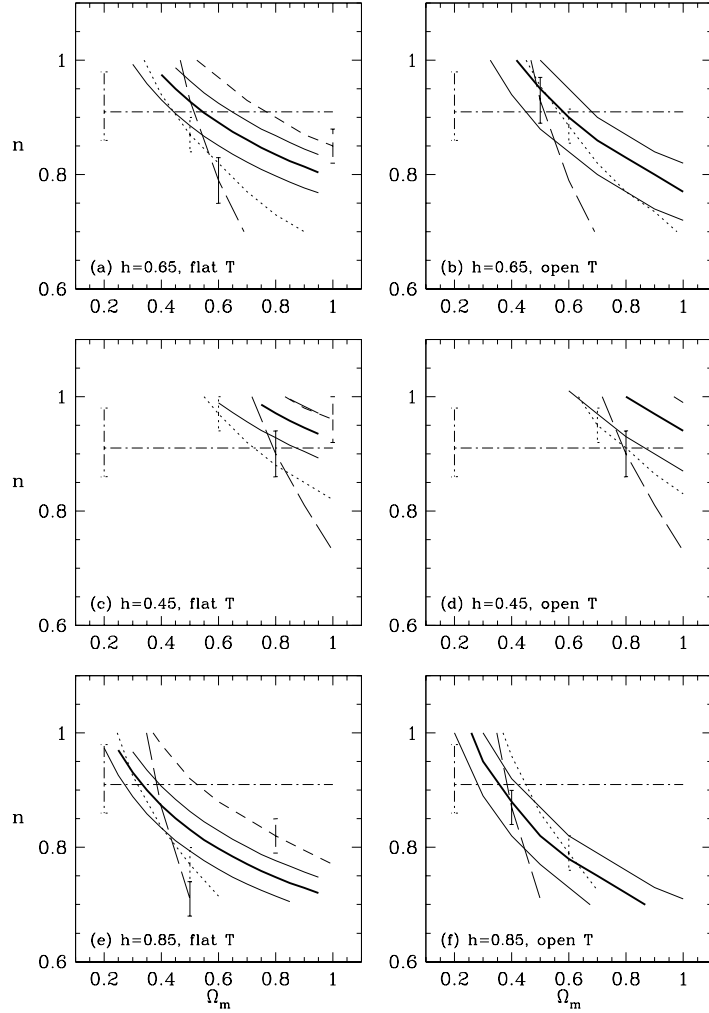


Fig. 5.— Like Figure 4, but for models with tensor fluctuations. Note that there is no version of the velocity power spectrum constraint for  $\Lambda$ CDM2. The CMB constraint on  $n$  does not impose the condition  $T/S = 7(1 - n)$ , but all of the other constraints do assume this condition and therefore cannot be applied for  $n > 1$ .

where  $\mu$ ,  $\nu$ ,  $k$  and  $\epsilon$  are dependent on the cosmology and  $h_{60} \equiv h/0.6$ . In a flat,  $\Omega_\Lambda = 1 - \Omega_m$  model with no tensor component,  $(\mu, \nu, k, \epsilon) = (1.3, 2.0, 0.58, 0.08)$ , while if a tensor component is allowed they become  $(1.3, 3.9, 0.58, 0.08)$ . For an open,  $\Omega_\Lambda = 0$  model without a tensor component they are  $(0.9, 1.4, 0.68, 0.07)$ . Freudling et al. (1998) do not consider open,  $\Omega_\Lambda = 0$  cases with a tensor component. For specified  $h$ , equation (10) yields a constraint in the  $\Omega_m - n$  plane, shown by the short-dashed line in the panels of Figures 4 and 5. The associated  $1\sigma$  error bars are based on the statistical uncertainties  $\epsilon$  quoted by Freudling et al. (1998) and listed above. For brevity, we will refer to these curves as the velocity power spectrum constraint, though they represent the constraints on the density power spectrum implied by peculiar velocities.

We do not want to use the amplitude of the galaxy power spectrum as one of our constraints because it can be strongly affected by biased galaxy formation. However, a variety of analytic and numerical arguments (e.g., Coles 1993; Fry & Gaztañaga 1993; Mann, Peacock, & Heavens 1998; Scherrer & Weinberg 1998; Narayanan, Berlind, & Weinberg 2000) suggest that biased galaxy formation should not alter the *shape* of the galaxy power spectrum on scales in the linear regime, and on these scales the shape is directly related to the parameters of the inflationary CDM cosmology. We adopt the specific constraint found by Peacock & Dodds (1994) from their combined analysis of a number of galaxy clustering data sets:

$$\Gamma_{\text{eff}} \equiv \Omega_m h \exp \left[ -\Omega_b \left( 1 + \frac{\sqrt{2h}}{\Omega_m} \right) \right] - 0.32 \left( \frac{1}{n} - 1 \right) = 0.255 \pm 0.017. \quad (11)$$

For  $n = 1$ ,  $\Gamma_{\text{eff}} = \Gamma$ , where  $\Gamma$  is the shape parameter in the conventional parameterization of the inflationary CDM power spectrum (Bardeen et al. 1986; the influence of  $\Omega_b$  is discussed by Sugiyama 1995). While the effects of  $\Gamma$  and  $n$  on the power spectrum shape are different, equation (11) combines them in a way that approximates their nearly degenerate influence over the range of scales currently probed by large scale clustering measurements. For specified  $h$  and  $B$ , equation (11) becomes a constraint in the  $\Omega_m - n$  plane. We plot this constraint as the long-dashed line and associated error bar in the panels of Figures 4 and 5. We should note, however, that the Peacock & Dodds (1994) error bar may be overoptimistic, since independent estimates of  $\Gamma_{\text{eff}}$  often fall outside this range. Eisenstein & Zaldarriaga (2001) have recently re-examined the spatial power spectrum inferred from the APM survey and conclude that the 68% confidence interval of  $\Gamma$  (for  $n = 1$ ) is  $0.19 - 0.37$ , much larger than the range implied by equation (11), and Efstathiou & Moody (2000) favor a lower central value ( $\Gamma \approx 0.12$ , with  $2\sigma$  range  $0.05 \leq \Gamma \leq 0.38$ ). As older estimates of the galaxy power spectrum are supplanted by results from the 2dF and Sloan galaxy redshift surveys, the  $\Gamma$  parameterization itself may become an insufficiently accurate representation of the theoretical predictions (Percival et al. 2001).

A detailed consideration of constraints from smaller scale CMB anisotropy measurements is beyond the scope of this paper, but we do want to draw on limits that smaller scale measurements place on the inflationary index  $n$ . For the no-tensor models, we adopt the “weak prior” constraint  $n = 0.96_{-0.09}^{+0.10}$  of Netterfield et al. (2001), based on data from the BOOMERANG experiment, which we represent by the horizontal dot-dash line and  $1\sigma$  error bar in Figure 4. Since Netterfield



et al. (2001) do not consider models with tensor fluctuations, we take the corresponding constraint for the tensor models in Figure 5 from Wang et al. (2001). Their model space is less restrictive than ours because they do not impose the power-law inflation relation  $T/S = 7(1 - n)$ , and using CMB data alone they find only a very weak constraint on  $n$ . We therefore adopt their constraint from the combination of CMB and large scale structure data,  $n = 0.91^{+0.07}_{-0.05}$ , where we have reduced the 95% confidence range quoted in their table 2 by a factor of two to get a representative  $1\sigma$  uncertainty.

In Figures 4 and 5, the cluster mass function, velocity power spectrum, and shape parameter constraints tend to be roughly parallel to each other, with the shape parameter following a somewhat different track when tensor fluctuations are important. The shape parameter constraint is usually compatible with the cluster mass function constraint, at least if one allows for the possibility that the error bar in equation (11) is somewhat too small. However, the velocity power spectrum always implies a higher fluctuation amplitude than the cluster mass function, and the two constraints are not consistent within their stated  $1\sigma$  uncertainties for any combination of  $\Omega_m$ ,  $n$ , and  $h$ . A recent analysis by Silberman et al. (2001) shows that the discrepancy is probably a result of non-linear effects on the velocity power spectrum, and that correcting for these yields results closer to the cluster constraint. We therefore regard the cluster constraint as more reliable, and we retain the velocity power spectrum curve mainly as a reminder of other data that can be brought to bear on these questions.

The  $\text{Ly}\alpha P(k)$  curve cuts across the other three constraints, requiring greater change in  $\Omega_m$  for a given change in  $n$ . The CMB anisotropy limit on  $n$  cuts across all of the other constraints. The COBE-DMR measurement is represented implicitly in Figures 4 and 5 through its role in the  $\text{Ly}\alpha P(k)$  constraint, the velocity power spectrum constraint, and the CMB anisotropy constraint on  $n$ . The size of the  $1\sigma$  error bars in these figures, and the probability that at least some of them are underestimated, prevents us from drawing sweeping conclusions. However, Figures 4 and 5 do have a number of suggestive implications if we look for models that lie within the overlapping  $1\sigma$  uncertainties of the various constraints. Since it is not possible to satisfy the cluster mass function and velocity power spectrum constraints simultaneously within the class of models that we consider, the implications depend strongly on which of these constraints we take to be more reliable. The shape parameter implications are usually intermediate, but significantly closer to those of the cluster mass function.

The combination of the velocity power spectrum and  $\text{Ly}\alpha P(k)$  constraints implies a high density universe, with  $\Omega_m \gtrsim 1$  preferred and  $\Omega_m \lesssim 0.6$  separating the two constraints by more than their  $1\sigma$  error bars. The  $\text{Ly}\alpha P(k)$  constraint rules out the high values of  $n$  that could otherwise allow low  $\Omega_m$  in equation (10). For  $h \geq 0.65$ , intersection of the velocity power spectrum and  $\text{Ly}\alpha P(k)$  constraints occurs at  $n \lesssim 0.8$ , incompatible with the CMB anisotropy constraint. However, an  $\Omega_m \sim 1$  universe would require a low value of  $h$  in any case because of the age constraint for globular cluster stars, and this would push the intersection to higher  $n$ . As noted earlier, the velocity power spectrum constraint shown here is probably biased towards high  $\Omega_m$  by

the non-linear effects described by Silberman et al. (2001).

If we instead adopt the cluster mass function constraint, then consistency with the Ly $\alpha$   $P(k)$  and COBE requires  $\Omega_m < 1$ . For  $h = 0.65$ , the constraints intersect at  $\Omega_m \sim 0.4 - 0.5$  in flat models and  $\Omega_m \sim 0.5 - 0.6$  in open models; increasing  $h$  slightly decreases the preferred  $\Omega_m$  and vice versa. This conclusion — that the combination of COBE, the Ly $\alpha$   $P(k)$ , and the cluster mass function implies a low density universe — is the most important and robust result to emerge from this multi-constraint analysis.

At one level, our conclusions about the matter density come as no surprise, since we have already argued, in Weinberg et al. (1999), that consistency between the cluster mass function and the Ly $\alpha$   $P(k)$  implies  $\Omega_m$  in this range independent of the COBE normalization. However, the nature of the argument is subtly different in this case. In Weinberg et al. (1999), we considered matter power spectra of the CDM form parameterized by  $\Gamma$  (with  $n = 1$ ), and by combining the Ly $\alpha$   $P(k)$  measurement with the cluster constraint (9), we found  $\Omega_m = 0.34 + 1.3(\Gamma - 0.2)$  for flat models and  $\Omega_m = 0.46 + 1.3(\Gamma - 0.2)$  for open models, with  $1\sigma$  uncertainties of about 0.1. However, the Ly $\alpha$   $P(k)$  alone could not rule out the solution of high  $\Omega_m$  and high  $\Gamma$ , so Weinberg et al.’s (1999) conclusion that  $\Omega_m < 1$  rested crucially on the empirical evidence for  $\Gamma \approx 0.2$  from the shape of the galaxy power spectrum. Within the class of CDM models considered here, the combination of COBE and the Ly $\alpha$   $P(k)$  determines  $n$ , and hence the effective value of  $\Gamma$  (eq. 11), once  $\Omega_m$ ,  $h$ , and  $B$  are specified. Simultaneous consistency between COBE, the Ly $\alpha$   $P(k)$ , and the cluster mass function requires low  $\Omega_m$  independent of the galaxy power spectrum shape, thereby strengthening the overall argument for a low density universe, and, by the by, for a matter power spectrum with low  $\Gamma_{\text{eff}}$ . The lower limit on  $\Omega_m$  from this combination of constraints varies with the choice of other parameters, but it never reaches as low as  $\Omega_m = 0.2$  unless  $h \geq 0.85$ .

For all of the models shown in Figures 4 and 5, the Ly $\alpha$   $P(k)$  and cluster mass function constraints intersect at values of  $n$  consistent with the CMB anisotropy constraints, provided one takes the  $1\text{-}\sigma$  error ranges into account. A factor of two improvement in the precision of the Ly $\alpha$   $P(k)$  measurement could greatly restrict the range of models compatible with all three constraints, especially if the Ly $\alpha$   $P(k)$  amplitude is somewhat lower, as McDonald et al. (2000) find.

There are, of course, numerous other constraints on cosmological parameters, and we will briefly consider three of them: the cluster baryon fraction, the location of the first acoustic peak in the CMB power spectrum, and the evidence for accelerating expansion from Type Ia supernovae. (Our focus on  $h = 0.65$  as a fiducial case already reflects our assessment of the most convincing direct estimates of  $H_0$ .) If one assumes that baryons are not overrepresented relative to their universal value within the virial radii of rich clusters, then the combination of the measured gas mass fractions with big bang nucleosynthesis limits on  $\Omega_b$  yields an upper limit on  $\Omega_m$  (White et al. 1993b). Applying this argument, Evrard (1997) concludes that

$$\Omega_m \Omega_b^{-1} h^{-3/2} \leq 23.1 \quad \implies \quad \Omega_m \leq 0.57 \left( \frac{B}{0.02} \right) \left( \frac{h}{0.65} \right)^{-1/2}, \quad (12)$$

at the 95% confidence level. From Figures 4 and 5 we see that models matching COBE, the Ly $\alpha$   $P(k)$ , and the cluster mass function are always consistent with this limit — easily in the case of flat models, sometimes marginally in the case of open models. Models that match the velocity power spectrum instead of the cluster mass function are usually incompatible with this limit, though sometimes only marginally so.

The location of the first acoustic peak in the CMB anisotropy spectrum is a strong diagnostic for space curvature (e.g., Doroshkevich, Zeldovich, & Sunyaev 1978; Wilson & Silk 1981; Sugiyama & Gouda 1992; Kamionkowski, Spergel, & Sugiyama 1994; Hu et al. 1997), and recent anisotropy measurements on degree scales favor a geometry that is close to flat (e.g., Miller et al. 1999; Melchiorri et al. 2000; Netterfield et al. 2001; Pryke et al. 2001). Clearly our flat universe models are compatible with these results, as are the open universe models that match the Ly $\alpha$   $P(k)$  and the velocity power spectrum (all of which have  $\Omega_m$  close to one). The open models that match Ly $\alpha$   $P(k)$  and the cluster mass function are generally ruled out by the most recent, high precision limits on space curvature. The Type Ia supernova measurements of the cosmic expansion history (Riess et al. 1998; Perlmutter et al. 1999) add a great deal of discriminatory power, since they constrain a parameter combination that is roughly  $\Omega_m - \Omega_\Lambda$  instead of  $\Omega_m + \Omega_\Lambda$ ; Perlmutter et al. (1999) quote  $\Omega_m - 0.75\Omega_\Lambda \approx -0.25 \pm 0.125$ . All of the open models miss this constraint by many  $\sigma$ , and the flat models matching the Ly $\alpha$   $P(k)$  and the velocity power spectrum fail because the values of  $\Omega_m$  are too high. The combination of COBE, the Ly $\alpha$   $P(k)$ , and the cluster mass function, on the other hand, is compatible with the supernova results for flat models with a cosmological constant, though it favors somewhat higher values of  $\Omega_m$ .

We have not carried out a similar multi-constraint analysis for the CHDM model because the formulas (11) and (10) for the shape parameter and velocity power spectrum constraints do not apply to it and the formula (9) for the cluster mass function constraint may be less accurate for non-zero  $\Omega_\nu$ . However, our fiducial CHDM model, with  $\Omega_\nu = 0.2$ , has  $\sigma_8 = 0.96$ , with  $n = 1.10$ . For  $\Omega_\nu = 0.3$  we obtain  $\sigma_8 = 1.15$  ( $n = 1.23$ ), for  $\Omega_\nu = 0.1$  we obtain  $\sigma_8 = 0.81$  ( $n = 0.96$ ), and for the TCDM model, which represents the limiting case of  $\Omega_\nu = 0$ , we obtain  $\sigma_8 = 0.77$  ( $n = 0.84$ ). All of these models are likely to violate the cluster mass function constraint, which according to equation (9) implies  $\sigma_8 = 0.52 \pm 0.04$  for  $\Omega_m = 1$ . We conclude that COBE-normalized CHDM models with  $\Omega_m = 1$ ,  $h \approx 0.5$  cannot simultaneously match the Ly $\alpha$   $P(k)$  and the cluster mass function. The Ly $\alpha$   $P(k)$  strengthens the case against this class of CHDM models by ruling out the low values of  $n$  that would otherwise allow them to match cluster masses (Ma 1996). Of course CHDM models with  $\Omega_m < 1$  can satisfy the observational constraints for appropriate parameter choices, and the general problem of using CMB measurements and the Ly $\alpha$   $P(k)$  to measure  $\Omega_\nu$  is discussed by Croft, Hu, & Davé (1999). However, the possible presence of a neutrino component does not alter our conclusion that COBE, the Ly $\alpha$   $P(k)$ , and the cluster mass function together require a low density universe.

All in all, the CWPHK and McDonald et al. (2000) measurements of the Ly $\alpha$   $P(k)$  provide additional support for the current “consensus” model of structure formation,  $\Lambda$ CDM with  $\Omega_m \approx 0.4$

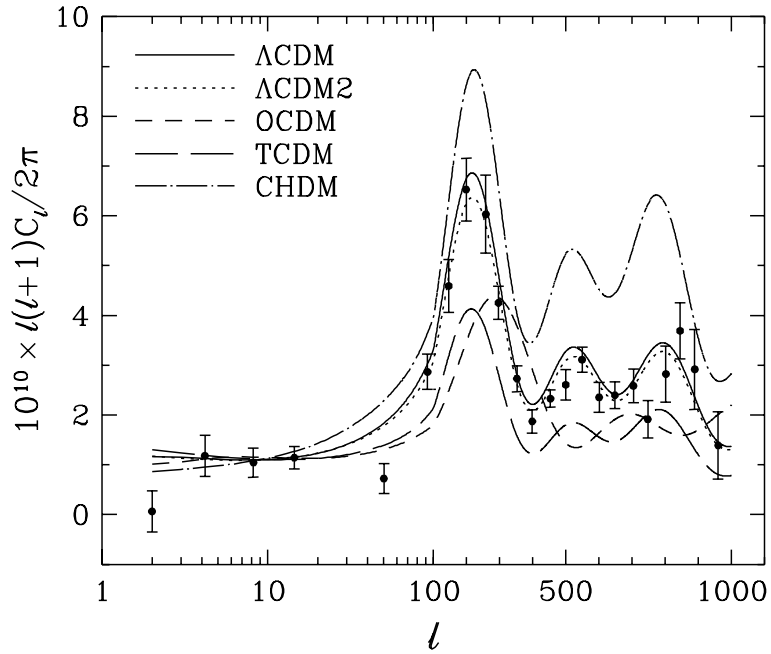


Fig. 6.— CMB anisotropy power spectra for five of the fiducial models that match COBE-DMR and the Ly $\alpha$   $P(k)$ .  $C_\ell$  is the mean-squared amplitude of spherical harmonics of order  $\ell$ . The models shown are  $\Lambda$ CDM (solid),  $\Lambda$ CDM2 (dotted), OCDM (long-dashed), TCDM (short-dashed), and CHDM (dot-dashed). Parameters of the models are listed in Table 1. Data points with  $1\sigma$  errors are taken from Wang et al. (2001). We shift from logarithmic spacing to linear spacing at  $\ell = 100$  in order to show both large and small angular scales clearly.

and  $h \approx 0.65$ . Moderate improvements in the statistical precision of the constraints considered here could strengthen this support, or they could open fissures of disagreement. Improvements in the near future could also allow some interesting new tests, such as discriminating between models with no tensor fluctuations and models with the  $T/S = 7(1 - n)$  contribution predicted by power law inflation.

A detailed consideration of the constraints from CMB anisotropy measurements is a major undertaking in itself, well beyond the scope of this paper. However, to illustrate the interplay between our results and recent CMB experiments, we plot in Figure 6 the predicted CMB power spectra of five of our fiducial models:  $\Lambda$ CDM,  $\Lambda$ CDM2, OCDM, TCDM, and CHDM. We computed these power spectra using CMBFAST (Seljak & Zaldarriaga 1996; Zaldarriaga, Seljak, & Bertschinger 1998), with the cosmological parameter values listed in Table 1. The CHDM model stands out from the rest because matching the Ly $\alpha$   $P(k)$  requires a high value of  $n$ , which boosts the anisotropy on small scales. The OCDM model also stands out, albeit less dramatically, because the open space geometry shifts the acoustic peaks to smaller angles. The TCDM model lies below the  $\Lambda$ CDM models because of its larger tilt, which suppresses small scale fluctuations. Figure 6 shows data points taken from the joint analysis of numerous CMB data sets by Wang et al. (2001; see their Table 1). The two  $\Lambda$ CDM models fit these data points remarkably well, given that the choice of their parameters was not based on small scale CMB data at all. Because the combination of COBE and the Ly $\alpha$   $P(k)$  implies  $n$  close to one for both of these models, their predictions are not very different, and the current CMB data do not distinguish between them. However, the TCDM, OCDM, and CHDM models are clearly ruled out, and while we have not attempted to adjust their parameters within the constraints allowed by equations (7) and (8), it appears unlikely that any such adjustment would allow these models to fit the current CMB data.

## 5. Conclusions

The slope of the mass power spectrum inferred by CWPHK from the Ly $\alpha$  forest,  $\nu = -2.25 \pm 0.18$  at  $k_p = 0.008 \text{ (km s}^{-1}\text{)}^{-1}$  at  $z = 2.5$ , confirms one of the basic predictions of the inflationary CDM scenario: an approximately scale-invariant spectrum of primeval inflationary fluctuations ( $n \approx 1$ ) modulated by a transfer function that bends the power spectrum towards  $P(k) \propto k^{n-4}$  on small scales. If the measured slope of the power spectrum had implied  $\nu > -2$  or  $\nu < -2.5$ , we would have been unable to reproduce the Ly $\alpha$   $P(k)$  with any of the models considered here, even allowing wide variations in the cosmological parameters.

Because the amplitude of the COBE-normalized power spectrum on small scales is very sensitive to  $n$ , we are able to match the CWPHK measurement of  $\Delta^2(k_p)$  in most of the major variants of the CDM scenario ( $\Lambda$ CDM, OCDM, TCDM, CHDM) by treating  $n$  as a free parameter. Within each of these variants, we obtain constraints on the model parameters of the form  $\Omega_m h^\alpha n^\beta B^\gamma = k \pm \epsilon$  (eq. 7) or  $\Omega_m h^\alpha n^\beta B^\gamma \Omega_\nu^\delta = k \pm \epsilon$  (eq. 8), with the parameter values listed in

Table 2. These constraints, together with the confirmation of the predicted slope, are the main results to emerge from combining the Ly $\alpha$   $P(k)$  measurement with the COBE-DMR result.

As shown in Figures 4 and 5, the parameter combination constrained by COBE and the Ly $\alpha$   $P(k)$  is different from the combinations constrained by other measurements of large scale structure and CMB anisotropy, so joint consideration of these constraints can break some of the degeneracies among the fundamental parameters. If we combine the Ly $\alpha$   $P(k)$  constraint with the constraint on  $\Omega_m$  and  $\sigma_8$  inferred from the cluster mass function (White et al. 1993a; ECF), then we favor a low density universe, with  $\Omega_m \sim 0.3 - 0.5$  in flat models and  $\Omega_m \sim 0.5 - 0.6$  in open models. This combination is also consistent with CMB anisotropy constraints on  $n$ . The open models are inconsistent with the angular location of the first acoustic peak in the CMB power spectrum (Netterfield et al. 2001; Pryke et al. 2001), and they are strongly inconsistent with Type Ia supernova results, which imply  $\Omega_m - 0.75\Omega_\Lambda \approx -0.25 \pm 0.125$  (Riess et al. 1998, Perlmutter et al. 1999). The flat models are consistent with both constraints. On the whole, the CWPBK measurement of the Ly $\alpha$   $P(k)$  supports the consensus in favor of  $\Lambda$ CDM with  $\Omega_m \approx 0.4$ ,  $h \approx 0.65$ . The contribution of the Ly $\alpha$   $P(k)$  to this consensus comes both from the slope, which confirms the generic inflationary CDM prediction, and from the amplitude, which has a different dependence on cosmological parameters than any of the other constraints considered here.

There are bright prospects for improvements of this approach in the near future. McDonald et al. (2000) have inferred the mass power spectrum from an independent Ly $\alpha$  forest data set using a different analysis method, obtaining a nearly identical slope and an amplitude lower by  $\sim 1\sigma$ . We have recently analyzed a much larger data set of high and moderate resolution spectra, using a variant of the Croft et al. (1998, 1999) method, and the improved data yield much higher statistical precision and better tests for systematic effects. Constraints from this new measurement of  $P(k)$ , using the method developed here, are presented in §7 of Croft et al. (2001). Recent measurements of CMB anisotropy have greatly improved the level of precision on small angular scales, and results from the MAP satellite should provide another major advance in the near future. These measurements yield tighter cosmological parameter constraints on their own, but they become substantially more powerful when combined with data that constrain the shape and amplitude of the matter power spectrum. It is evident from Figures 4 and 5 that simply reducing the error bars on  $n$  and the Ly $\alpha$   $P(k)$  by a factor of two would already produce interesting new restrictions on the allowable range of models. These restrictions can become very powerful if ongoing studies of cluster masses using galaxy dynamics, X-ray properties, the Sunyaev-Zel'dovich effect, and gravitational lensing confirm the robustness of the cluster mass function constraint. In the slightly longer term, the 2dF and Sloan redshift surveys should produce measurements of the shape of the galaxy power spectrum that shrink the current statistical and systematic uncertainties, so that demanding consistency between the inferred value of  $\Gamma_{\text{eff}}$  and other constraints becomes a useful additional test. At the very least, these developments should lead to a powerful test of the inflationary CDM picture and high-precision determinations of its parameters. If we are lucky, improved measurements will reveal deficiencies of the simplest  $\Lambda$ CDM

models that are hidden within the current uncertainties, and resolving these discrepancies will lead us to a better understanding of the cosmic energy contents and the origin of primordial fluctuations in the hot early universe.

We thank Daniel Eisenstein and Wayne Hu for helpful advice on computing power spectra, Martin White for comments on the manuscript, and Nikolay Gnedin for a prompt and helpful referee’s report. This work was supported by NASA Astrophysical Theory Grants NAG5-3111, NAG5-3922, and NAG5-3820, by NASA Long-Term Space Astrophysics Grant NAG5-3525, and by NSF grants AST-9802568, ASC 93-18185, and AST-9803137.

## REFERENCES

- Bahcall, N. A., Ostriker, J. P., Perlmutter, S., & Steinhardt, P. J. 1999, *Science*, 284, 1481
- Bardeen, J., Bond, J. R., Kaiser, N., & Szalay, A. 1986, *ApJ*, 304, 15
- Bennett, C., L., Banday, A. J., Gorski, K. M., Hinshaw, G., Jackson, P., Keegstra, P., Kogut, A., Smoot, G. F., Wilkinson, D. T., & Wright, E. L. 1996, *ApJ*, 646, L1
- Bi, H.G., & Davidsen, A. 1997, *ApJ*, 479, 523
- Bond, J. R., & Efstathiou, G. 1991, *Phys Lett B*, 265, 245
- Bridle, S. L., Eke, V. R., Lahav, O., Lasenby, A. N., Hobson, M. P., Cole, S., Frenk, C. S., & Henry, J. P. 1999, *MNRAS*, 310, 565
- Bunn, E. F., & White, M. 1997, *ApJ*, 480, 6
- Burles, S., & Tytler, D. 1997, *AJ*, 114, 1330
- Burles, S., & Tytler, D. 1998, *ApJ*, 507, 732
- Cen, R., Miralda-Escudé, J., Ostriker, J.P., & Rauch, M. 1994, *ApJ*, 437, L9
- Coles, P., 1993, *MNRAS*, 262, 1065
- Croft, R. A. C., Hu, W., & Davé, R. 1999a, *Phys Rev Lett*, 83, 1092
- Croft, R. A. C., Weinberg, D. H., Katz, N., & Hernquist, L. 1998, *ApJ*, 495, 44
- Croft, R. A. C., Weinberg, D. H., Bolte, M., Burles, S., Hernquist, L., Katz, N., Kirman, D., Tytler, D. 2001, *ApJ*, submitted, astro-ph/0012324
- Croft, R. A. C., Weinberg, D. H., Pettini, M., Katz, N., & Hernquist, L. 1999b, *ApJ*, 520, 1 (CWPHK)
- Davis, R. L., Hodges, H. M., Smoot, G. F., Steinhardt, P. J., & Turner, M. S. 1992, *Phys Rev Lett*, 69, 1856
- Doroshkevich, A. G., Zeldovich, Ya. B., & Sunyaev, R. A. 1978, *Sov Astron*, 22, 523
- Efstathiou, G., Bond, J. R., & White, S. D. M. 1992, *MNRAS*, 258, 1p
- Efstathiou, G., & Moody, S. J. 2000, *MNRAS*, submitted, astro-ph/0010478
- Eisenstein, D. J., & Hu, W. 1999, *ApJ*, 511, 5
- Eisenstein, D. J., & Zaldarriaga, M. 2001, *ApJ*, 546, 2
- Eke, V. R., Cole, S., & Frenk, C. S. 1996, *MNRAS*, 282, 263 (ECF)



- Evrard, A. E. 1997, MNRAS, 292, 289
- Freudling, W., Zehavi, I., da Costa, L.N., Dekel, A., Eldar, A., Giovanelli, R., Haynes, M. P., Salzer, J.J., Wegner, G. & Zaroubi, S. 1999, ApJ, 523, 1
- Fry, J. N., & Gaztañaga, E. 1993, ApJ, 413, 447
- Hernquist L., Katz, N., Weinberg, D.H., & Miralda-Escudé, J. 1996, ApJ, 457, L5
- Hu, W., Sugiyama, N., & Silk, J. 1997, Nature, 386, 37
- Hu, W., & White, M. 1997, ApJ, 486, L1
- Hui, L., Gnedin, N., & Zhang, Y. 1997, ApJ, 486, 599
- Kamionkowski, M., Spergel, D. N., & Sugiyama, N. 1994, ApJ, 426, L57
- Kates, R., Müller, V., Gottlöber, S., Mücke, J. P., & Retzlaff, J. 1995, MNRAS, 277, 1254
- Ma, C. 1997, ApJ, 471, 13
- Mann, R. G., Peacock, J. A., & Heavens, A. F. 1998, MNRAS, 293, 209
- McDonald, P., Miralda-Escudé, J., Rauch, M., Sargent, W. L. W., Barlow, T. A., Cen, R., & Ostriker, J. P. 2000, ApJ, 543, 1
- Melchiorri, A. et al. 2000, ApJ, 536, L63
- Miller, A. D. et al. 1999, ApJ, 524, L1
- Mould, J. R., et al. 2000, ApJ, 545, 547
- Narayanan, V. K., Berlind, A. A., & Weinberg, D. H. 2000, ApJ, 528, 1
- Netterfield, C. B., et al. 2001, ApJ, submitted, astro-ph/0104460
- Novosyadlyj, B., Durrer, R., Gottlöber, S., Lukash, V. N., & Apunevych, S. 2000, A&A, 356, 418
- Peacock, J. A., & Dodds, S. J. 1994, MNRAS, 267, 1020
- Peebles, P. J. E., & Ratra, B. 1998, ApJ, 325, L17
- Percival, W. J., et al. 2001, MNRAS, in press, astro-ph/0105252
- Perlmutter, S., et al. 1999, ApJ, 517, 565
- Press, W. H., & Schechter, P. 1974, ApJ, 187, 425
- Pryke, C., Halverson, N. W., Leitch, E. M., Kovac, J., Carlstrom, J. E., Holzzapfel, W. L., & Dragovan, M. 2001, ApJ, submitted, astro-ph/0104490

- Riess, A. G., et al. 1998, *AJ*, 116, 1009
- Sachs, R. K., & Wolfe, A. M. 1967, *ApJ*, 147, 73
- Scherrer, R. J., & Weinberg, D. H. 1998, *ApJ*, 504, 607
- Seljak, U., & Zaldarriaga, M. 1996, *ApJ*, 469, 437
- Silberman, L., Dekel, A., Eldar, A., & Zehavi, I. 2001, *ApJ*, in press, astro-ph/0101361
- Smoot, G. F., et al. 1992, *ApJ*, 396, L1
- Steigman, G., Hata, N., & Felten, J. E. 1999, *ApJ*, 510, 564
- Sugiyama, N. 1995, *ApJS*, 100, 281
- Sugiyama, N., & Gouda, N. 1992, *Prog Theor Phys*, 88, 803
- Tegmark, M. 1999, *ApJ*, 514, L69
- Walker, T.P., Steigman, G., Schramm, D.N., Olive, K.A., & Kang, H.S 1991, *ApJ*, 376, 51
- Wang, L., & Steinhardt, P. J. 1998, *ApJ*, 508, 483
- Wang, X., Tegmark, M., & Zaldarriaga, M. 2001, *Phys. Rev. D*, submitted, astro-ph/0105091
- Weinberg, D. H., Croft, R. A. C., Hernquist, L., Katz, N., & Pettini, M. 1999, *ApJ*, 522, 563
- White, S. D. M., Efstathiou, G. P., & Frenk, C. S. 1993a, *MNRAS*, 262, 1023
- White, S. D. M., Navarro, J. F., Evrard, A. E., & Frenk, C. S. 1993b, *Nature*, 366, 429
- Wilson, M. S., & Silk, J. 1981, *ApJ*, 243, 14
- Zaldarriaga, M., Seljak, U., & Bertschinger, E. 1998, *ApJ*, 494, 491
- Zhang, Y., Anninos, P., & Norman, M.L. 1995, *ApJ*, 453, L57